

# Learning Interpretable Logic Rules from Deep Vision Models

Chuqin Geng  
McGill University

chuqin.geng@mail.mcgill.ca

Haolin Ye  
McGill University

haolin.ye@mail.mcgill.ca

Yuhe Jiang  
University of Toronto

yuhe.jiang@mail.utoronto.ca

Zhaoyue Wang  
McGill University

zhaoyue.wang@mail.mcgill.ca

Ziyu Zhao  
McGill University

ziyu.zhao2@mail.mcgill.ca

Xujie Si  
University of Toronto

six@cs.toronto.edu

## Abstract

We propose a general framework called *VisionLogic* to extract interpretable logic rules from deep vision models, with a focus on image classification tasks. Given any deep vision model that uses a fully connected layer as the output head, *VisionLogic* transforms neurons in the last layer into predicates and grounds them into vision concepts using causal validation. In this way, *VisionLogic* can provide local explanations for single images and global explanations for specific classes in the form of logic rules. Compared to existing interpretable visualization tools such as saliency maps, *VisionLogic* addresses several key challenges, including lack of causal explanations, overconfidence in visualizations, and ambiguity in interpretation. *VisionLogic* also facilitates the study of visual concepts encoded by predicates, particularly how they behave under perturbation—an area that remains underexplored in the field of hidden semantics. Apart from providing better visual explanations and insights into the visual concepts learned by the model, we show that *VisionLogic* retains most of the neural network’s discriminative power in an interpretable and transparent manner. We envision it as a bridge between complex model behavior and human-understandable explanations, providing trustworthy and actionable insights for real-world applications.

## 1. Introduction

While deep learning-based vision models have achieved remarkable success, their black-box nature remains a significant challenge. This issue is further emphasized by the recent shift from convolutional neural networks (CNNs) [13, 17] to Vision Transformers (ViTs) [7], highlighting the growing complexity and opacity of modern architectures.

To this end, we propose a general framework called *VISIONLOGIC* to extract interpretable logic rules from deep vision models, with a focus on image classification tasks.

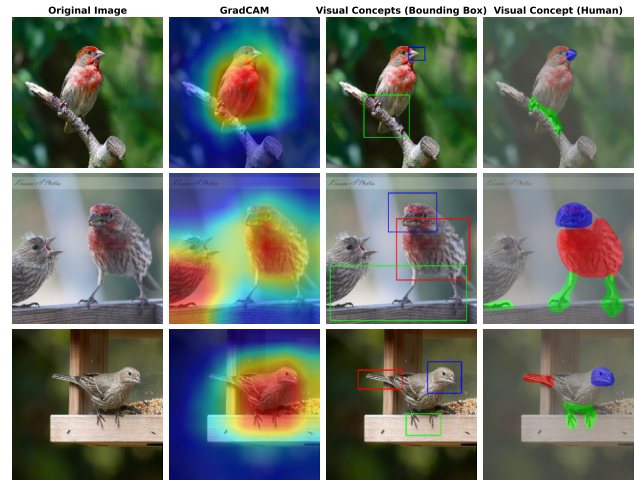


Figure 1. Comparison of *VISIONLOGIC* and GradCAM: *VISIONLOGIC* is capable of identifying individual visual concepts with bounding boxes; human annotations can further refine and highlight the regions activating the predicates.

Given any deep vision model that uses a fully connected (FC) layer as the output head — a common architecture for both CNNs and transformers — *VISIONLOGIC* transforms neurons from the fully connected layer into predicates. This enables the framework to learn both local explanations for single images and global explanations for specific classes in the form of logic rules. Our experiments on both ResNet and ViT demonstrate that *VISIONLOGIC* explains models’ decision-making processes in an interpretable and transparent manner, while retaining most of the neural network’s discriminative power, as supported by achieving over 80% top-5 validation accuracy.

To further enhance interpretability, we ground hidden predicates into high-level visual concepts using causal inference. Specifically, we first use bounding boxes to build causal mappings between certain image regions and predicates across a collection of images belonging to the same

class. This is achieved through an ablation study, where regions are cropped and replaced with random noise to determine whether the predicate flips from *True* to *False*. We then leverage human input to identify consistent visual concepts within those bounding boxes. In this way, VISIONLOGIC achieves both human alignment and causal validation, ensuring that the extracted rules are both faithful and interpretable. In contrast, existing work on hidden semantics [3, 23] lacks causal evidence and tends to capture spurious correlations.

As VISIONLOGIC provides local explanations and enables attribution to the input space, it can serve as a powerful visual explanation tool, similar to saliency maps [5, 25]. Unlike saliency maps, which produce heatmap-like outputs that often overemphasize local features, VISIONLOGIC highlights entire regions containing meaningful visual concepts, as illustrated in Figure 1. For these highlighted regions, our visual concepts are supported by causal evidence, whereas saliency maps often suffer from false confidence and misleading explanations [30]. Furthermore, VISIONLOGIC offers explanations of image predictions in the form of interpretable logic rules. For example, it can express relationships such as “*Beak*”  $\wedge$  “*Claw*”  $\Rightarrow$  “*Bird*”, as shown in Figure 1. This capability of generating logic-based explanations is a unique feature not supported by saliency methods.

VISIONLOGIC also facilitates the study of visual concepts encoded by predicates, particularly how they behave under perturbation. As a whole, it helps us understand how vision models behave under various kinds of scene changes or adversarial attacks. Finally, we summarize our contributions as follows:

- We present a novel framework, VISIONLOGIC, for extracting interpretable rules from deep vision models. VISIONLOGIC provides local and global explanations in the form of logic rules while retaining most of the neural network’s discriminative power.
- We ground hidden predicates to high-level visual concepts using bounding boxes and human annotations. Our approach is both faithful and interpretable, leveraging causal inference to avoid spurious correlations.
- We demonstrate that predicates encoding visual concepts exhibit interesting properties, such as many-to-many mappings, capturing both local parts and global structures, along with robustness to adversarial attacks.
- We conduct thorough experiments to evaluate both the local and global explanations generated by VISIONLOGIC. Our experiments include both objective and subjective assessments, highlighting its advantages over existing interpretable methods and approaches.

## 2. Related Work

Numerous approaches have been proposed to address the interpretability of vision models. One major line of work

focuses on saliency maps, which attribute a model’s predictions to specific input features. Notable methods in this area include Grad-CAM [25], which uses gradient information flowing into the final convolutional layer to produce coarse localization maps; Grad-CAM++ [5], an extension of Grad-CAM that improves localization accuracy by considering higher-order gradients; and Score-CAM [30], which replaces gradients with channel-wise weights to reduce noise and improve interoperability. Despite providing straightforward visual explanations, saliency map methods suffer from several key limitations. For instance, they can be independent of both the data and the model that was trained on [1]. Another issue is false confidence, where activation maps with higher weights may contribute less to the network’s output [30]. Furthermore, saliency maps are often limited to single inputs and tend to overemphasize local features [35].

Another line of research focuses on hidden semantics [3, 9, 21, 23], which attempts to explain a hidden neuron or layer by associating visual concepts with their activations. However, they often lack causal evidence, as they primarily rely on observing co-occurrences between visual concepts and neuron activations [4, 34]. As a result, the method is less reliable and prone to capturing spurious correlations. Furthermore, despite their merits, neither saliency maps nor hidden semantics provide an effective way to interpret the decision-making process of neural networks in a manner that is intuitive for humans.

Earlier work on logic rule extraction from neural networks dates back to the pre-deep learning era of the 1990s [10, 26–28], and was therefore developed for relatively small datasets, such as the Iris dataset. These approaches primarily adapt search techniques for combinations of specific value ranges in input attributes, cluster the activation values of hidden neurons, and perform layer-by-layer rule generation and rewriting. However, they face scalability challenges, making them especially unsuitable as neural networks become deeper in modern applications. As a result, more recent “rule as explanation” methods shift toward local interpretability on individual samples [31, 33].

Our approach preserves the advantage of the above three lines of work, while attempting to avoid their limitations. It provides logic rules as local and global explanations, which are highly interpretable to humans, but operates only on the last FC layer to mitigate scalability challenges. By grounding predicates to visual concepts using causal inference and human-in-the-loop alignment, it addresses the issue of spurious correlations. As a visual explanation tool, it also avoids several key limitations, such as being restricted to single inputs, false confidence, and saturating gradients [30]. We envision VISIONLOGIC as a powerful framework for bridging the gap between complex model behavior and human-understandable explanations, enhancing trust-

worthiness and understanding in deep vision models.

### 3. The VISIONLOGIC Framework

Modern deep vision models, such as ResNet [13] and ViT [7], typically employ a single fully connected layer as the output layer to generate final predictions in classification tasks. While prior research [2, 32] has recognized the significance of the final decision layer, these studies primarily focus on analyzing its sparsity and robustness, rather than deriving explicit, interpretable rules. In this work, we address this gap by proposing VISIONLOGIC, a framework that approximates the final layer using logic rules. Our approach can be further decomposed into the following steps.

#### 3.1. Deriving predicates from neuron activations

The first challenge is to construct a set of predicates  $P$  that describe specific properties of the input sample  $x$ . A predicate  $p_j(x)$  evaluates to a truth value if the corresponding property is satisfied. A natural starting point is to leverage the neurons in the final FC layer  $\mathbf{F}$ , as their activations encode discriminative features essential for classification. To transform these activations into predicates, we must determine thresholds that convert continuous activation values into Boolean outputs.

However, a key question arises: *how can we compute an optimal threshold for each neuron to retain the discriminative power of the neural network?* Finding an exact solution is challenging due to the combinatorial nature of the problem and the complexity of the decision boundary. To address this, we propose a simple yet efficient approximation method. Recall that the prediction score for an input  $x$  belonging to class  $c$  is given by  $\mathbf{F}^c(x) = \mathbf{W}^c \mathbf{Z}(x) + \mathbf{b}^c$ , where  $\mathbf{Z}(x)$  represents the activations of the neurons in the last layer. For  $x$  to be classified as  $c$ ,  $\mathbf{F}^c(x)$  must be the highest among all classes. A neuron  $j$  is considered most representative for class  $c$  if its average contribution, measured by the average ranking of  $\mathbf{W}_j^c \mathbf{Z}_j(x)$  among all neurons  $j \in J$ , is the highest, with higher rankings closer to 1, across a set of inputs  $x \in X$ . Formally, this can be expressed as:

$$j = \arg \min_{j \in J} \mathbb{E}_{x \in X} [\mathcal{R}^c(\mathbf{W}_j^c \mathbf{Z}_j(x))], \quad (1)$$

where  $\mathcal{R}^c(\mathbf{W}_j^c \mathbf{Z}_j(x))$  denotes the ranking of the contribution of neuron  $j$  relative to all other neurons  $j \in J$  for a given input  $x$  in class  $c$ . For models using the ReLU activation function (which are non-negative) [22], the threshold  $T_j$  for neuron  $j$  is computed as follows. First, we collect the activation values  $\mathbf{Z}_j$  for instances that meet the following criteria: (1) they are *correctly classified* as class  $c$ , where neuron  $j$  is deemed most representative, and (2) neuron  $j$  has the highest contribution among all neurons for these instances. The threshold  $T_j$  is then defined as the minimum

activation value within this set. The predicate  $p_j(x)$  evaluates to True if:

$$p_j(x) := \mathcal{I}(\mathbf{z}_j(x) \geq T_j), \quad (2)$$

where  $\mathcal{I}(\cdot)$  is the indicator function that returns 1 (True) if the condition is satisfied and 0 (False) otherwise. If the set is empty, set the threshold to a large value so that  $p_j(x)$  is always *False*. We call such a predicate *invalid*. In contrast, a **valid** predicate can output either True or False.

For more general activation functions like GELU [14], which produce activations over  $(-\infty, \infty)$ , both the positive and negative branches of activations can be essential for representing certain classes. To account for this, we create two predicates:  $p_{j,+}$  and  $p_{j,-}$ . To compute the threshold for  $p_{j,+}$ , we collect the activation values  $\mathbf{Z}_j$  from instances that satisfy the following conditions: (1) they are *correctly classified* as class  $c$ , where neuron  $j$  is considered most representative, constrained by  $\mathbf{W}_j^c > 0$ ; and (2) neuron  $j$  has the highest contribution among all neurons for these instances. The threshold  $T_{j,+}$  is then defined as the minimum activation value within this set. Similarly, for  $p_{j,-}$ , we collect activation values  $\mathbf{Z}_j$  on instances where  $j$  ranks first in contribution for its most representative class  $c$ , constrained by  $\mathbf{W}_j^c < 0$ . The threshold  $T_{j,-}$  is then set as the maximum activation value in this set. The predicates  $p_{j,+}(x)$  and  $p_{j,-}(x)$  evaluate to True if:

$$p_{j,+}(x) := \mathcal{I}(\mathbf{z}_j(x) \geq T_{j,+}), \quad p_{j,-}(x) := \mathcal{I}(\mathbf{z}_j(x) \leq T_{j,-})$$

respectively, where  $\mathcal{I}(\cdot)$  is the indicator function.

#### 3.2. Learning logic rules from deep vision models

Given an input  $x$  and a set of predicates  $P$ , we generate a *local explanation* for  $x$  by constructing a logical expression using predicates from  $P$  combined with the logical connective  $\wedge$ , denoted as  $P(x)$ . Each predicate  $p_j \in P$  evaluates to True or False based on  $x$ , and the logical expression combines these evaluations into an interpretable decision rule.

To learn a global explanation for a class  $c$ , we adopt a data-driven approach. Specifically, we feed all training data from class  $c$  into the set of predicates  $P$  and collect their corresponding activation patterns. For example, suppose we have three predicates  $p_1, p_2, p_3$  (omitting  $x$  for clarity), and five distinct inputs yield the following patterns:  $(0, 1, 1)$ ,  $(1, 1, 0)$ ,  $(1, 1, 0)$ ,  $(1, 0, 1)$ , and  $(1, 0, 1)$ . We then use the logical connective  $\vee$  to create a disjunction of the distinct conjunctive forms, deriving a rule:

$$\forall x \quad (p_2 \wedge p_3) \vee (p_1 \wedge p_2) \vee (p_1 \wedge p_3) \Rightarrow \text{Label}(x) = c.$$

While such formalism provides an accurate description of class  $c$ , it can exhibit poor generalization to unseen test data due to overfitting. To address this, we employ a

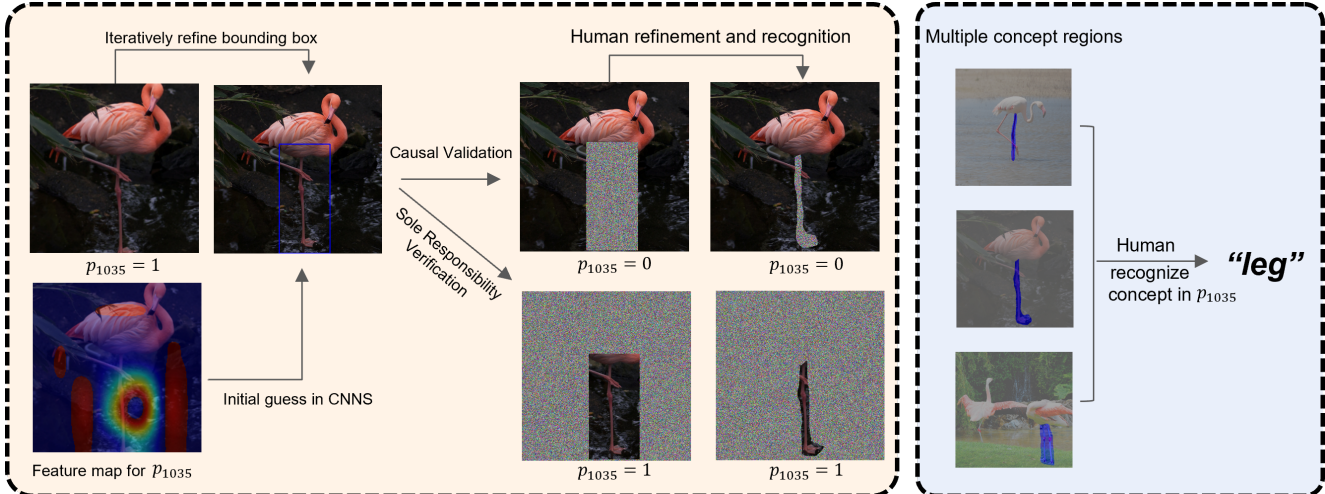


Figure 2. Grounding hidden predicates to high-level visual concepts. We iteratively refine the bounding box to localize potential regions containing visual concepts. These regions are validated to: 1) causally affect a specific predicate  $p_j$ , and 2) be solely responsible for computing  $p_j$ . Human annotators further refine these regions and recognize consistent visual concepts across multiple such regions.

ranking-based scoring method rather than exact rule matching, enabling more flexible and robust reasoning.

For a given class  $c$ , we collect all predicates appearing in the logical expressions derived from its training data. Let  $P^c$  denote the set of predicates for class  $c$ , sorted in descending order of their frequency.  $P^c$  can be considered as *global explanation* for class  $c$ . We say a class  $c$  can *explain* a certain input  $x$  if the predicates in  $P(x)$  form a subset of  $P^c$ . However, since predicates can be shared among many classes, there may be multiple classes that can *explain* a given input  $x$ . Suppose we are not given any ground truth – is it possible to find the most plausible class that best explains the input  $x$ ?

To this end, we define an *explanation score*  $S(x, c)$  to measure the explanatory power of class  $c$  for  $x$ . This score is computed as the average ranking of predicates in  $P(x)$  with respect to  $P^c$ :

$$S(x, c) = \frac{1}{|P(x)|} \sum_{p_j \in P(x)} \mathcal{R}^c(p_j), \quad (3)$$

where  $\mathcal{R}^c(p_j)$  is the ranking function for class  $c$ , and  $|P(x)|$  is the number of predicates in  $P(x)$ . A higher average ranking indicates higher confidence in the explanatory power, as it reflects the presence of more representative predicates for class  $c$ . Finally, the class  $c$  with the lowest explanation score (highest rank) is selected as the best explanation for  $x$ .

Compared to neural networks, VISIONLOGIC achieves greater interpretability through logical expressions and explanation scores, offering a transparent and human-understandable decision-making process.

### 3.3. Grounding predicates to vision concepts

The next challenge is to ground these predicates in the input space, linking abstract logic to tangible input features. However, since inputs undergo complex transformations before being mapped to predicates, tracing how these predicates define decision boundaries is highly challenging. To address this, we ground predicates in high-level visual concepts rather than raw input features. This idea aligns with research on hidden semantics [4, 29, 34].

For an input image  $x$ , we assess whether specific regions significantly contribute to the computation of predicate  $p_j(x)$ . This is achieved by cropping the region of interest, filling it with random noise, and processing the modified image  $x'$  through the model to compute  $p_j(x')$ . A transition of  $p_j$  from activation to deactivation provides causal evidence that the identified region is crucial for  $p_j(x)$ . To locate such regions more efficiently and precisely, we employ an algorithm that starts with an initial bounding box guess designed to deactivate  $p_j$ . This initial guess is typically a large box cropping out most part of the image; in CNNs, it can be derived from the feature map of  $p_j$ . The algorithm then iteratively refines the bounding box until  $p_j$  becomes activated, following a methodology similar to that in [11].

For ViT and its variants, since images are already processed using fixed-size patches, we can leverage these patches during refinement. Due to the stochastic nature of the refinement process, the algorithm may produce varying bounding boxes across trials. To enhance the precision of localizing potential visual concepts, we select the smallest bounding box from these trials. Additionally, we verify that the region is solely responsible for computing  $p_j$  by con-

structuring an image composed of random noise, retaining only the region of interest, and confirming that it still activates  $p_j$ . For more precise localization of potential visual concepts, we leverage human annotators to draw flexible regions that closely align with the boundaries of the visual concepts present in the image. Figure 2 illustrates the entire workflow.

To identify the visual concepts encoded by predicate  $p_j$ , we apply this approach to detect regions of interest across multiple images. Human annotators then analyze these regions to identify consistent visual concepts, establishing a robust causal relationship between the concepts and  $p_j$ . In contrast, existing research in hidden semantics often associates visual concepts with neurons by observing their co-occurrence [4, 34], a method that is less reliable and prone to capturing spurious correlations.

## 4. Experiments

We conduct a comprehensive set of experiments to evaluate both the local and global explanations generated by VISIONLOGIC. Our experiments include both objective and subjective assessments, as detailed in this section. To demonstrate the generalizability of our approach across different models and to compare the performance of CNN and Transformer architectures, we will cover the following deep vision models: ResNet-50 [13], ConvNet-Base [19], ViT-B [7], and Swin-T [18]. For the dataset, we use the ImageNet validation dataset [6], which consists of 50,000 images.

### 4.1. Assessing global interpretability

We evaluate how effectively VISIONLOGIC preserves the neural network’s decision-making process and discriminative power, as well as the complexity of the logic rules it generates for individual samples and classes. To quantify these aspects, we define the following metrics:

- **Number of valid predicates (Valid.):** The total number of valid predicates generated by VISIONLOGIC.
- **Local explanation complexity (Local.):** The average number of predicates in the local explanation for images.
- **Global explanation complexity (Global.):** The average number of predicates in the global explanation for classes.
- **Coverage (Cover.):** The percentage of total images that can be explained by the ground truth with VISIONLOGIC.
- **Agreement ratio (Agree.):** The percentage of total images where VISIONLOGIC agree with the prediction outcome of the neural network.
- **Top-1 accuracy:** The percentage of images where VISIONLOGIC’s top-1 class matches the ground truth.
- **Top-5 accuracy:** The percentage of images where the ground truth is among VISIONLOGIC’s top-5 classes.

Table 1 summarizes the evaluation of the interpretability of VISIONLOGIC across various models using the proposed

metrics. As demonstrated, trained on the ImageNet’s train-set, VISIONLOGIC exhibits strong generalization ability to unseen validation data. If ground truth is accessible, VISIONLOGIC can explain over 80% of the validation data for both CNNs and Transformers. When ground truth is unavailable, it can serve as a logic-based version of a neural network, achieving competitive accuracy. For instance, on ConvNet, it achieves 67.30% and 81.45% top-1 and top-5 accuracy, respectively. Given that it can only explain 83.77% of the total data, the performance after correction improves to 80.33% and 97.23% for top-1 and top-5 accuracy, respectively — even outperforming its neural network counterpart. It is noteworthy that, although VISIONLOGIC is trained exclusively on positive examples, it still correctly identifies about 5% of the images misclassified by neural networks. This is evident from the difference between the Agreement Ratio and Top-1 Accuracy. In other words, VISIONLOGIC can match false predictions with rules, offering insights into misclassification causes and helping investigate model robustness under perturbations and adversarial attacks, as shown in Section 4.4.

For the model-wise comparison, we observe that CNNs tend to generate shorter explanations for both images and classes compared to Transformers. For example, ResNet requires an average of 9.49 and 567.40 predicates to explain image samples and classes, while Swin Transformer necessitates an average of 53.58 and 1226.54 predicates, despite having more active predicates overall (1944 vs. 1460). Our observation aligns with recent work [15], which suggests “disjunctive“ behaviors (rule-like structures) within CNNs and “compositional“ behaviors in ConvNeXt and Transformers, explained by having more predicates in our case. However, this work only uses indirect evidence, such as sub-explanation counting, rather than explicitly extracting rules. *To the best of our knowledge, VISIONLOGIC is the first work to achieve this explicit extraction.* We leave further improvements in accuracy as future work, with the primary challenge being the enhancement of coverage.

### 4.2. Assessing local interpretability

As the primary approach for local interpretability involves visual explanation rather than logical rules, we evaluate the local interpretability of VISIONLOGIC using visual explanations and compare it with baseline methods such as Grad-CAM, Grad-CAM++, and Score-CAM. Since our method generates bounding boxes instead of assigning saliency scores to individual pixels, we adopt the metrics proposed in [16]: *loc1* and *loc5*. These metrics consider a result correct if the intersection over union (IoU) between the estimated and ground-truth bounding boxes is at least 0.5, with *loc1* requiring the top-1 prediction to be correct and *loc5* considering the top 5 predictions. The evaluation is conducted on 2000 images sampled from the ILSVRC validation set (with

Table 1. Evaluation of VISIONLOGIC’s interpretability across various models, including both CNNs and Transformers. The first column lists the models, while the remaining columns report results based on the proposed metrics. The values in parentheses under **Valid.** indicate the total number of predicates, while those under **Top-1 Acc.** and **Top-5 Acc.** show the original neural network accuracy.

Model	Valid.	Local.	Global.	Cover. (%)	Agree. (%)	Top-1 Acc. (%)	Top-5 Acc. (%)
ResNet	1944 (2048)	9.49	567.40	83.48	62.21	57.83 (80.86)	78.08 (95.43)
ConvNet	1303 (2048)	33.75	825.34	83.77	<b>72.10</b>	<b>67.30</b> (83.76)	<b>81.45</b> (96.87)
ViT	1465 (1536)	42.63	1077.11	80.48	70.46	64.95 (81.07)	78.37 (95.32)
Swin	1460 (1536)	53.58	1226.54	<b>88.64</b>	69.67	64.56 (81.47)	80.90 (95.78)

ground-truth bounding boxes) [24], using ResNet. VISIONLOGIC uses the bounding box from the highest-ranking predicate, which typically captures the most dominant part of the image. In contrast, baseline methods generate bounding boxes based on the approach in [16].

Table 2. Comparison of localization accuracy.

Metric (%)	Grad-CAM	Grad-CAM++	Score-CAM	VISIONLOGIC
<i>loc1</i>	46.25	49.89	44.70	<b>53.59</b>
<i>loc5</i>	54.51	58.35	55.13	<b>64.19</b>

Table 2 summarizes the results, demonstrating that VISIONLOGIC outperforms existing methods in localization accuracy. Unlike Grad-CAM, Grad-CAM++, and Score-CAM, which may exhibit false confidence, VISIONLOGIC leverages causal validation for more reliable and precise localization. By identifying essential structural elements, it aligns more closely with human annotations, leading to improved localization performance. These results underscore VISIONLOGIC’s effectiveness in providing interpretable and robust visual explanations.

### 4.3. Understanding visual concepts in predicates

We present human-interpretable visual concepts encoded by predicates found in both ResNet and ViT. Each judgment is supported by many examples, with only a few case analyses shown in Figure 3 as a summary. The 2<sup>nd</sup> and 4<sup>th</sup> rows present examples from ViT, while the remaining rows show examples from ResNet. The sampled concepts include “squirrel’s head”, “squirrel’s tail (or paws)”, “bird’s head”, “bird’s beak”, “fox’s ears”, and “church tops”.

#### Many-to-many mapping between predicates and concepts

It is observed that there is a many-to-many relationship between predicates and visual concepts. A single predicate can be deactivated when either (or both) of two distinct visual concepts are masked, meaning the predicate can encode multiple visual concepts, either within the same class or across different classes. Conversely, a single visual concept may be encoded by multiple predicates, such that masking the relevant region deactivates several predicates simultaneously.

An example of a single predicate encoding multiple concepts can be found in the 5<sup>th</sup> image of the first row, where both the tail and the paws of the squirrel are represented by  $p_{1916}$  from ResNet. Another instance is  $p_{1878}$ , which simultaneously encodes both “fox’s ears” and “church tops”. While these are distinct concepts, they share a similar triangular shape, which may explain why they are represented by the same predicate. A particularly interesting example is the predicate  $p_{489}$ , shown in the 3<sup>rd</sup> and 5<sup>th</sup> rows. This predicate is frequently used to encode the beak of birds, even across different species. We identified  $p_{489}$  in classes such as “jay,” “vulture”, and “kite,” as well as in many other local explanations generated from bird images, where it plays a crucial role during inference.

An example of a single concept encoded by multiple predicates can be found in the 5<sup>th</sup> and 6<sup>th</sup> rows: in the class “fox”, both  $p_{1878}$  and  $p_{170}$  encode the visual concept “fox’s ears”. It is worth noting that a predicate can attend to multiple instances of the same visual concept within an image. For example, in the 3<sup>rd</sup> image of the 6<sup>th</sup> row, which contains two foxes,  $p_{1878}$  attends to the ears of both foxes. This suggests that these predicates serve as global concept detectors, highlighting a key advantage of the rule-based model we have extracted.

#### Predicates robustly identify visual concepts across variations in appearance

The human visual system can recognize objects belonging to the same concept despite significant differences in appearance, such as color and shape. Interestingly, our learned predicates exhibit a similar capability. For example, in the third row of Figure 3, the concept “bird’s head” appears from both the front and the side, yet  $p_{1890}$  consistently attends to it. Similarly,  $p_{1878}$  captures varying forms, sizes, and angles of “church tops”.

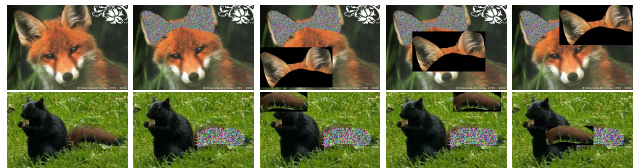


Figure 4. Sensitivity to location changes.



Figure 3. Hidden predicates grounded in visual concepts. Each predicate is supported by three images. In each image, the predicate is labeled above the image frame, and the colored region within the image highlights the concept identified by the human annotator.

**Sensitivity to location changes** Some predicates appear to be location-invariant, while others are not, as illustrated in Figure 4. Predicate  $p_{170}$  in the top row remains active even when the “fox’s ears” are shifted across the third, fourth, and fifth images. In contrast, predicate  $p_{1916}$  in the bottom row, which encodes “squirrel’s tail”, is deactivated once the tail moves away from its original position.

**Top-ranked predicates typically encode the global structure** In addition to the predicates that capture local and modular concepts discussed above, we also observe that some predicates capture the global structure. Figure 5 illustrates two examples from the classes “church” and “squirrel”, where  $p_{908}$ ,  $p_{(498,-)}$ ,  $p_{219}$ , and  $p_{(312,+)}$  from ResNet and ViT encode the entire structure of the church and the

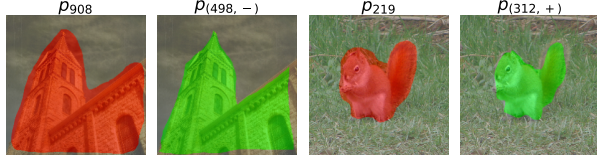


Figure 5. Predicates ranked first encode the global structure. Red regions correspond to ResNet, while green correspond to ViT.

squirrel, respectively. This is supported by causal evidence—masking out any modular concept in the image does not deactivate these predicates, but masking out the entire church or squirrel does.

Such predicates are typically top-ranked:  $p_{908}$ ,  $p_{(498,-)}$ ,  $p_{219}$ , and  $p_{(312,+)}$  all rank first in their respective classes. Additionally, we find that these global predicates are less shared across classes, meaning they tend to overfit to specific categories, whereas predicates encoding local concepts are more commonly shared between classes. This observation holds for both CNNs and Transformers.

**Comparison between CNNs and Transformers** Generally, similar concepts can be identified in both CNNs and Transformers, as shown in 1<sup>st</sup> and 2<sup>nd</sup> rows, where the predicates from both models are identified to capture the same visual concepts given the same image. However, a key difference is observed: Transformers tend to have more predicates encoding or being influenced by a single concept, while CNNs exhibit a more distinct encoding for each concept. We hypothesize the root causes as follows: 1) CNN models may utilize a greater total number of predicates compared to ViT models, 2) ReLU and GELU activations utilize different branches of activations into predicates, with ReLU seeming to encourage sparsity, and 3) the attention mechanism and convolution filters may have different priors in learning visual concepts and representations. We leave the validation of these hypotheses to future work.

#### 4.4. Probing robustness of vision models

We investigate the success of adversarial attacks through the lens of local explanations generated by VISIONLOGIC. From a logical rule perspective, misclassification typically occurs when (1) the top-ranked predicates of the ground truth class are deactivated, and (2) predicates associated with other classes become active. While these often co-occur, we define (1) as the root cause—denoted as a *Type I* cause—if it alone can alter the prediction without (2). Similarly, we define a *Type II* cause when (2) alone is sufficient to induce misclassification. These two causes are attack-agnostic, enabling us to understand the underlying logic behind different attacks.

We provide concrete examples in Figure 6. The original image follows the rule  $p_{669} \wedge p_{844} \wedge p_{489} \Rightarrow \text{“jay”}$ . After the



Figure 6. This displays the original image, followed by the images after PGD, Gaussian noise, and Pixelate attacks from left to right.

Table 3. Statistics of root causes under various adversarial attacks.

Attack	ResNet		ConvNet		ViT		Swin	
	Type I	Type II	Type I	Type II	Type I	Type II	Type I	Type II
Gaussian	79	921	116	884	149	851	109	891
Pixelate	214	786	329	671	267	733	298	702
PGD	377	623	561	439	653	347	612	388

PGD attack, the rule becomes  $p_{1220} \wedge p_{489} \wedge p_{537} \wedge p_{844} \Rightarrow \text{“tray”}$ , which is a Type II cause, as introducing the new predicate  $p_{1220}$  significantly increases the explanation score for the class “tray”. The Gaussian Noise attack yields  $p_{2032} \wedge p_{1074} \wedge p_{2028} \cdots \wedge p_{669} \wedge p_{844} \wedge p_{489} \Rightarrow \text{“badger”}$ , introducing many new predicates, which is a Type II cause. The Pixelation attack results in  $p_{2028} \wedge p_{376} \wedge p_{1940} \cdots \wedge p_{211} \Rightarrow \text{“black grouse”}$ , deactivating all original predicates, thus exhibiting a Type I cause.

To conduct a systematic evaluation, we randomly sample 1,000 images from the ImageNet validation set, applying a successful attack to each image once using Projected Gradient Descent (PGD) [20], Gaussian noise [12], and Pixelate attacks [8], respectively.

Table 3 presents the statistics of root causes across different adversarial attacks. The Gaussian noise attack tends to affect all active predicates simultaneously, often activating new predicates, which is primarily explained by Type II causes. The Pixelate attack operates similarly but has a higher chance of deactivating existing predicates, leading to more Type I causes, as it dilutes the fine-grained details of regions attended by the predicates. Finally, the PGD attack is the most efficient and selects either Type I or Type II causes to achieve the quickest result. For ResNet, which generates shorter explanations, it favors introducing new predicates. For transformers, which use more predicates in their explanations, it leans more toward deactivations. We aim to investigate more attacks and defenses in future work.

## 5. Conclusion and Future Work

In conclusion, VISIONLOGIC represents a significant step forward in making deep vision models interpretable and transparent. By transforming neurons in the last fully connected layer into predicates and grounding them into visual concepts through causal validation, VISIONLOGIC provides both local and global explanations as logical rules. For future work, we identify the following directions: 1) While

this work mainly focuses on interpretability with high-level vision concepts, a natural extension is to explore low-level features such as edges, corners, and textures. Can we identify logical rules with these more fundamental building blocks of objects? 2) VISIONLOGIC shows promising results in approximating neural network accuracy with interpretable, transparent rule-based models. Theoretically, when training on new images or addressing misclassified images, rule-based models benefit from “adding patches”, which do not require retraining on the entire dataset, as is necessary with neural networks. This approach suggests a new paradigm of efficient and debuggable learning.

## References

- [1] Julius Adebayo, Justin Gilmer, Michael Muelly, Ian Goodfellow, Moritz Hardt, and Been Kim. Sanity checks for saliency maps. *Advances in Neural Information Processing Systems*, 31, 2018. [2](#)
- [2] Debangshu Banerjee, Avaljot Singh, and Gagandeep Singh. Interpreting robustness proofs of deep neural networks. In *The Twelfth International Conference on Learning Representations, ICLR 2024, Vienna, Austria, May 7-11, 2024*. OpenReview.net, 2024. [3](#)
- [3] David Bau, Bolei Zhou, Aditya Khosla, Aude Oliva, and Antonio Torralba. Network dissection: Quantifying interpretability of deep visual representations. In *2017 IEEE Conference on Computer Vision and Pattern Recognition, CVPR 2017, Honolulu, HI, USA, July 21-26, 2017*, pages 3319–3327. IEEE Computer Society, 2017. [2](#)
- [4] David Bau, Jun-Yan Zhu, Hendrik Strobelt, Bolei Zhou, Joshua B. Tenenbaum, William T. Freeman, and Antonio Torralba. GAN dissection: Visualizing and understanding generative adversarial networks. In *7th International Conference on Learning Representations, ICLR 2019, New Orleans, LA, USA, May 6-9, 2019*. OpenReview.net, 2019. [2](#), [4](#), [5](#)
- [5] Aditya Chattopadhyay, Anirban Sarkar, Prantik Howlader, and Vineeth N Balasubramanian. Grad-cam++: Generalized gradient-based visual explanations for deep convolutional networks. *2018 IEEE Winter Conference on Applications of Computer Vision (WACV)*, pages 839–847, 2018. [2](#)
- [6] Jia Deng, Wei Dong, Richard Socher, Li-Jia Li, Kai Li, and Li Fei-Fei. Imagenet: A large-scale hierarchical image database. In *2009 IEEE conference on computer vision and pattern recognition*, pages 248–255. Ieee, 2009. [5](#)
- [7] Alexey Dosovitskiy, Lucas Beyer, Alexander Kolesnikov, Dirk Weissenborn, Xiaohua Zhai, Thomas Unterthiner, Mostafa Dehghani, Matthias Minderer, Georg Heigold, Sylvain Gelly, Jakob Uszkoreit, and Neil Houlsby. An image is worth 16x16 words: Transformers for image recognition at scale. *arXiv preprint arXiv:2010.11929*, 2021. [1](#), [3](#), [5](#)
- [8] Logan Engstrom, Andrew Ilyas, Shibani Santurkar, Dimitris Tsipras, Jacob Steinhardt, and Aleksander Madry. Robustness library. In *GitHub repository*, 2019. [8](#)
- [9] Ruth Fong and Andrea Vedaldi. Net2vec: Quantifying and explaining how concepts are encoded by filters in deep neural networks. In *Proceedings of the IEEE conference on computer vision and pattern recognition*, pages 8730–8738, 2018. [2](#)
- [10] LiMin Fu. Rule learning by searching on adapted nets. In *Proceedings of the 9th National Conference on Artificial Intelligence, Anaheim, CA, USA, July 14-19, 1991, Volume 2*, pages 590–595. AAAI Press / The MIT Press, 1991. [2](#)
- [11] Chuqin Geng, Zhaoyue Wang, Haolin Ye, Saifei Liao, and Xujie Si. Learning minimal NAP specifications for neural network verification. *CoRR*, abs/2404.04662, 2024. [4](#)
- [12] Ian Goodfellow, Yoshua Bengio, Aaron Courville, and Yoshua Bengio. *Deep learning*. MIT Press, 2016. [8](#)

- [13] Kaiming He, Xiangyu Zhang, Shaoqing Ren, and Jian Sun. Deep residual learning for image recognition. In *Proceedings of the IEEE conference on computer vision and pattern recognition*, pages 770–778, 2016. 1, 3, 5
- [14] Dan Hendrycks and Kevin Gimpel. Gaussian error linear units (gelus). *arXiv preprint arXiv:1606.08415*, 2016. 3
- [15] Mingqi Jiang, Saeed Khorram, and Li Fuxin. Comparing the decision-making mechanisms by transformers and cnns via explanation methods. In *Proceedings of the IEEE/CVF Conference on Computer Vision and Pattern Recognition*, pages 9546–9555, 2024. 5
- [16] Peng-Tao Jiang, Chang-Bin Zhang, Qibin Hou, Ming-Ming Cheng, and Yunchao Wei. Layercam: Exploring hierarchical class activation maps for localization. *IEEE Trans. Image Process.*, 30:5875–5888, 2021. 5, 6
- [17] Yann LeCun, Léon Bottou, Yoshua Bengio, and Patrick Haffner. Gradient-based learning applied to document recognition. *Proceedings of the IEEE*, 86(11):2278–2324, 1998. 1
- [18] Ze Liu, Yutong Lin, Yue Cao, Han Hu, Yixuan Wei, Zheng Zhang, Stephen Lin, and Baining Guo. Swin transformer: Hierarchical vision transformer using shifted windows. *Proceedings of the IEEE/CVF International Conference on Computer Vision (ICCV)*, pages 10012–10022, 2021. 5
- [19] Zhuang Liu, Hanzi Mao, Chao-Yuan Wu, Christoph Feichtenhofer, Trevor Darrell, and Saining Xie. A convnet for the 2020s. In *IEEE/CVF Conference on Computer Vision and Pattern Recognition, CVPR 2022, New Orleans, LA, USA, June 18-24, 2022*, pages 11966–11976. IEEE, 2022. 5
- [20] Aleksander Madry, Aleksandar Makelov, Ludwig Schmidt, Dimitris Tsipras, and Adrian Vladu. Towards deep learning models resistant to adversarial attacks. In *6th International Conference on Learning Representations, ICLR 2018, Vancouver, BC, Canada, April 30 - May 3, 2018, Conference Track Proceedings*. OpenReview.net, 2018. 8
- [21] Aravindh Mahendran and Andrea Vedaldi. Understanding deep image representations by inverting them. In *Proceedings of the IEEE conference on computer vision and pattern recognition*, pages 5188–5196, 2015. 2
- [22] Vinod Nair and Geoffrey E Hinton. Rectified linear units improve restricted boltzmann machines. pages 807–814, 2010. 3
- [23] Anh Nguyen, Alexey Dosovitskiy, Jason Yosinski, Thomas Brox, and Jeff Clune. Synthesizing the preferred inputs for neurons in neural networks via deep generator networks. *Advances in neural information processing systems*, 29, 2016. 2
- [24] Olga Russakovsky, Jia Deng, Hao Su, Jonathan Krause, Sanjeev Satheesh, Sean Ma, Zhiheng Huang, Andrej Karpathy, Aditya Khosla, Michael S. Bernstein, Alexander C. Berg, and Li Fei-Fei. Imagenet large scale visual recognition challenge. *Int. J. Comput. Vis.*, 115(3):211–252, 2015. 6
- [25] Ramprasaath R Selvaraju, Michael Cogswell, Abhishek Das, Ramakrishna Vedantam, Devi Parikh, and Dhruv Batra. Grad-cam: Visual explanations from deep networks via gradient-based localization. *International Journal of Computer Vision*, 128(2):336–359, 2017. 2
- [26] Rudy Setiono and Huan Liu. Understanding neural networks via rule extraction. In *Proceedings of the Fourteenth International Joint Conference on Artificial Intelligence, IJCAI 95, Montréal Québec, Canada, August 20-25 1995, 2 Volumes*, pages 480–487. Morgan Kaufmann, 1995. 2
- [27] Rudy Setiono and Huan Liu. Neurolinear: From neural networks to oblique decision rules. *Neurocomputing*, 17(1):1–24, 1997.
- [28] Geoffrey G. Towell and Jude W. Shavlik. Extracting refined rules from knowledge-based neural networks. *Mach. Learn.*, 13:71–101, 1993. 2
- [29] Andrey Voynov and Artem Babenko. Unsupervised discovery of interpretable directions in the GAN latent space. In *Proceedings of the 37th International Conference on Machine Learning, ICML 2020, 13-18 July 2020, Virtual Event*, pages 9786–9796. PMLR, 2020. 4
- [30] Haofan Wang, Mengnan Du, Fan Yang, and Zifan Zhang. Score-cam: Score-weighted visual explanations for convolutional neural networks. *Proceedings of the IEEE/CVF Conference on Computer Vision and Pattern Recognition Workshops*, pages 24–25, 2020. 2
- [31] Tong Wang. Gaining free or low-cost interpretability with interpretable partial substitute. In *Proceedings of the 36th International Conference on Machine Learning, ICML 2019, 9-15 June 2019, Long Beach, California, USA*, pages 6505–6514. PMLR, 2019. 2
- [32] Eric Wong, Shibani Santurkar, and Aleksander Madry. Leveraging sparse linear layers for debuggable deep networks. In *Proceedings of the 38th International Conference on Machine Learning, ICML 2021, 18-24 July 2021, Virtual Event*, pages 11205–11216. PMLR, 2021. 3
- [33] Mike Wu, Sonali Parbhoo, Michael C. Hughes, Ryan Kindle, Leo A. Celi, Maurizio Zazzi, Volker Roth, and Finale Doshi-Velez. Regional tree regularization for interpretability in deep neural networks. In *The Thirty-Fourth AAAI Conference on Artificial Intelligence, AAAI 2020, The Thirty-Second Innovative Applications of Artificial Intelligence Conference, IAAI 2020, The Tenth AAAI Symposium on Educational Advances in Artificial Intelligence, EAAI 2020, New York, NY, USA, February 7-12, 2020*, pages 6413–6421. AAAI Press, 2020. 2
- [34] Ceyuan Yang, Yujun Shen, and Bolei Zhou. Semantic hierarchy emerges in deep generative representations for scene synthesis. *Int. J. Comput. Vis.*, 129(5):1451–1466, 2021. 2, 4, 5
- [35] Bolei Zhou, Aditya Khosla, Agata Lapedriza, Aude Oliva, and Antonio Torralba. Learning deep features for discriminative localization. *Proceedings of the IEEE Conference on Computer Vision and Pattern Recognition*, pages 2921–2929, 2016. 2